Chapter 5

M^3 System for Viscous Drag Reduction

In aerospace engineering, drag reduction is one of the most challenging problems of aircraft. Drag limits the maximum speed, the maximum range of flight and the operational cost. For example, reduction of the drag by a few percent can amount to billions of dollars of annual savings world wide on commercial aircraft fuel cost. There are three types of drags - pressure or form drag, drag due to lift and skin-friction or viscous drag. The pressure drag involves the viscous influence upon the ideal or inviscid-flow pressure field. It is generally small in the attached flow cases but increases tremendously when flow separation occurs. Therefore, the foremost consideration for drag control is to avoid flow separation, which in most cases can be achieved by simply streamlining the body shape. The drag due to lift is caused by flow spillage on lifting surfaces from high- to low-pressure regions. Skin-friction drag is the result of the no-slip boundary condition on the wall and exists in both laminar and turbulent flows. It is equal to the integral of shear stress over the object surface area. Therefore the skin-friction drag in turbulent flow is higher than that in laminar flow. When the flow is attached, it is usually the major contributor to the total drag. For this reason, the reduction of skin-friction drag has been actively pursued by many researchers and will be the subject of study in this chapter.

5.1 Skin-Friction Drag Reduction

It has been known for more than a decade that a surface of grooves, known as riblets, can reduce skin-friction drag through the interaction with the sub-layer streaky structures in turbulent flows if the groves are aligned to the mean flow direction [1,2,3]. Optimally,

as much as 8% of drag reduction has been achieved [4]. Several flight tests performed have also confirmed the drag reduction performance of riblets. Since the riblets have to be in the inner layer (sub-layer) of the boundary layer in order to for the riblets to be effective, they are called internal manipulators. In contrast to the riblets, the large eddy break-up devices (LEBUs) which extend from the surfaces to the outer layer are known as external manipulators or outer layer devices. They can “calm” the flow passing them, thus reducing the drag [5,6]. These two types of manipulators are all *passive* control means for drag reduction because there are no adaptation of the surface to flow. One serious problem with these techniques is that they only work for a narrow velocity range.

In addition to the passive means, a number of researchers have also explored the *active* means for reducing turbulent drags. These include the mass transport through porous walls [7], selective suction and blowing derived from the drag reduction mechanism on a shark’s skin [7,8,9,10], and actuator movements [11,12]. The numerical simulations (CFD) have predicted that the *interactive* drag reduction scheme, i.e. the closed-loop feedback control systems with a large amount of distributed sensors and actuators with sizes comparable to the turbulent structures, can be much more effective than the passive means [7]. However, the experimental realization of such micro systems was not possible until just recently when MEMS technology is developed and introduced to flow control.

5.2 MEMS Skin-Friction Drag Reduction Approach

High skin-friction drag in a turbulent flow is caused by the counter-rotating vortex pairs which bring high momentum fluids down to the wall and create local high shear stress streaks. The basic mechanism of our MEMS skin-friction drag reduction approach is to pump the high momentum fluids in the vortices away from the wall by moving the surface-mounted micro-flaps up and down, thus reducing the surface shear stress. This concept has been proved by hot-wire measurements in the 2-D laminar flow section of the wind-tunnel described in Chapter 4, where a vortex generator is placed on the wall to

induce a stationary vortex pair and a micro-actuator is placed down-stream of the vortex generator [13,14,15]. In Figure 5.1, the drag coefficients (defined as the drag force normalized to the dynamic force) derived from hot-wire measurements are plotted against the phase of the actuator excited by sine waves at different frequencies. It can be seen that the drag coefficients with actuator movements are always lower than that without actuator. In fact, under certain condition (e.g., actuator in the up position at the frequency of 40 Hz), the drag coefficient is even lower than that without the vortex generator, i.e. when the flow is laminar.

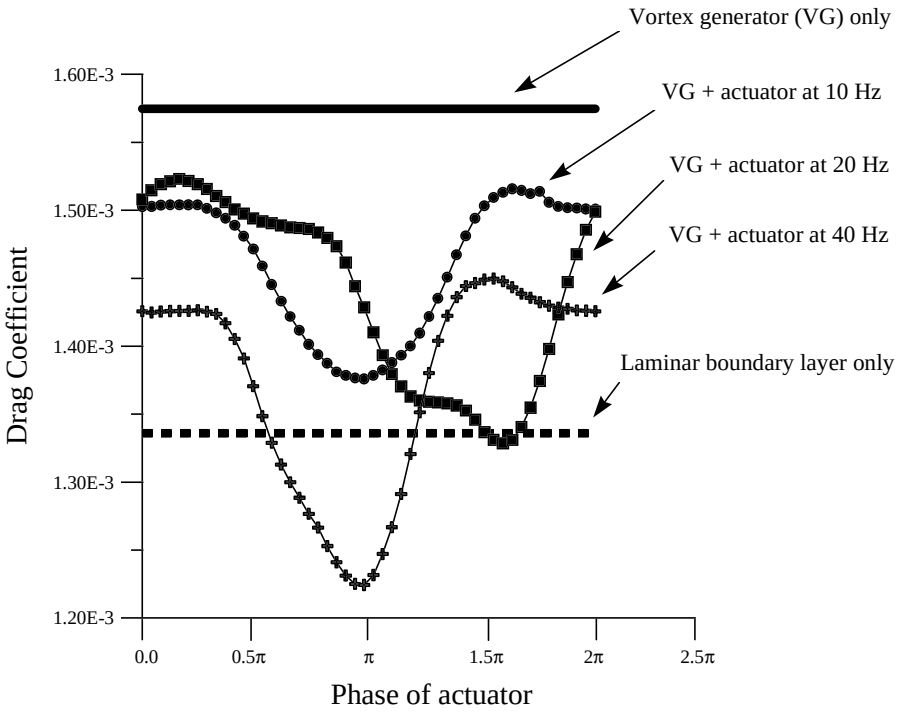

Figure 5.1 Drag coefficient (defined as the normalized drag force to dynamic force) change with the phase of the actuator excited by sine wave with different frequencies.

In addition to the hot-wire measurement, a hybrid MEMS control system using individual actuator, shear stress sensors, and integrated CMOS circuits fabricated through MOSIS is under way to directly confirm the drag reduction capability in fully developed turbulent flows [16].

5.3 System Integration

In the mean time of the drag reduction study using the hybrid system, we are exploring the possibility of integrating the micro-sensors, micro-actuators and microelectronics (M^3) on a single Si chip and eventually making a complete distributed micro-system for drag reduction on a Si wafer. We have developed a technology for the integration of the three different types of devices and the prototype M^3 chips have been fabricated by using this technology, as shown in Figure 5.2. The chip consists of three basic flow control units in parallel. Each unit uses one surface micromachined magnetic actuator with torsional support beams [16]. There are three shear stress sensors biased at constant temperature mode on the upstream of the actuator for measuring the passing sub-layer structures. Their outputs are amplified and then fed to a CMOS edge detector [17,18]. If a high shear stress streak is identified, the edge detector will send a signal to activate the driver of the actuator and the driver then outputs a sinusoidal current to oscillate the actuator. The other three shear stress sensors on the downstream of the actuator are only used to check the effect of the actuation.

The integration process of the CMOS circuits, shear stress sensors and magnetic actuators is far more complex than the sum of the individual processes. First, the CMOS process has to be finished before any MEMS devices are fabricated because of its strict requirement on the wafer cleanness and surface condition. Second, aluminum metallization for the CMOS devices can not be done until all the high temperature (> 450^oC) materials are deposited. Third, the processing temperature during the fabrication of the MEMS devices can not exceed 950^oC in order to prevent the change on the doping profiles of the fabricated CMOS transistors. This has ruled out the possibility of having a separate LOCOS just for MEMS devices. Finally, certain masking materials other than photoresist are needed to protect the structures that are not being processed during various sacrificial layer etchings (high-concentration HF etch, TMAH etch, etc.).

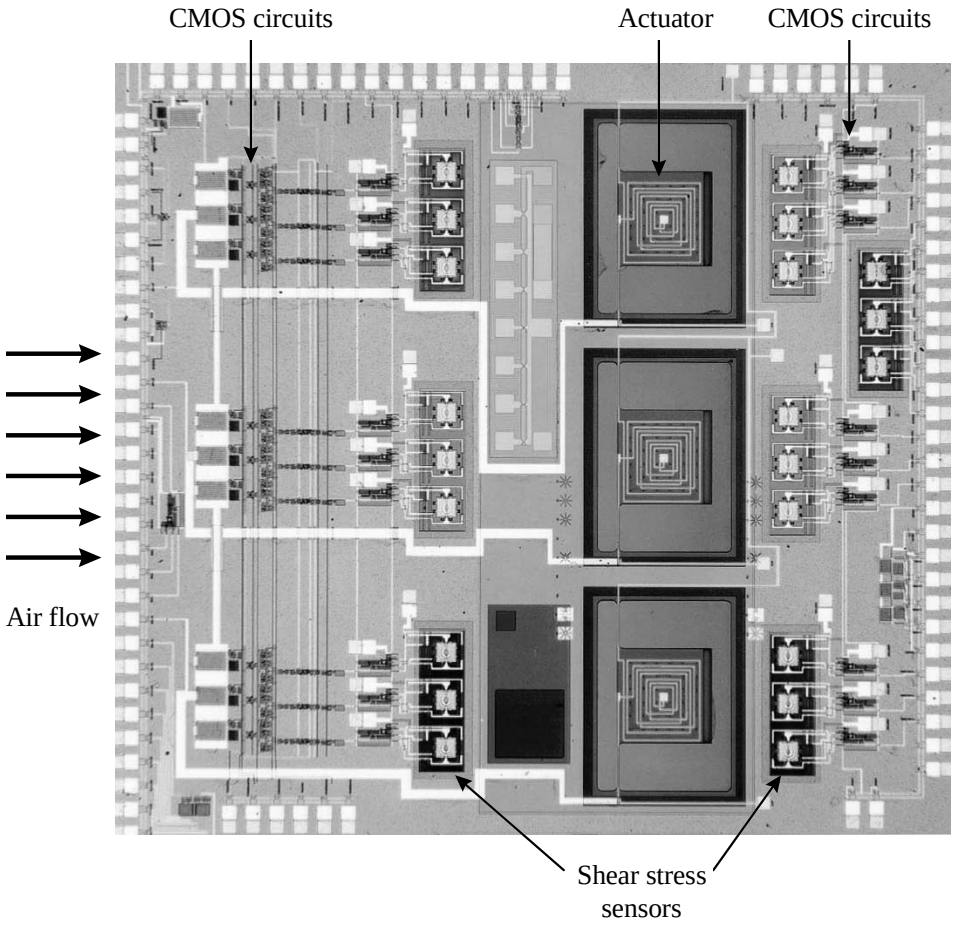

Figure 5.2 A 1×1 cm^2 prototype M^3 chip with integrated shear stress sensors, micro magnetic actuators and CMOS control circuits.

Based on the above considerations, we have designed the process for the fabrication of the prototype M^3 chips, which is described in Appendix A. Totally, the process includes 22 masking steps. The simplified process flow with cross-sections are shown in Figure 5.3. The baseline CMOS process steps up to the deposition of PSG are finished in the Microlab of the University of California at Berkeley. The wafers are then sent to our lab for the fabrication of the shear stress sensors and the processing of the high temperature materials for the actuators. Metallization for the CMOS circuits and the shear stress sensors are completed in Berkeley. Finally, we finish the low temperature processing steps for the actuators, including the deposition and patterning of LTO and chrome/gold, and the sacrificial layer (polysilicon) etching in TMAH and BrF_3 [16].

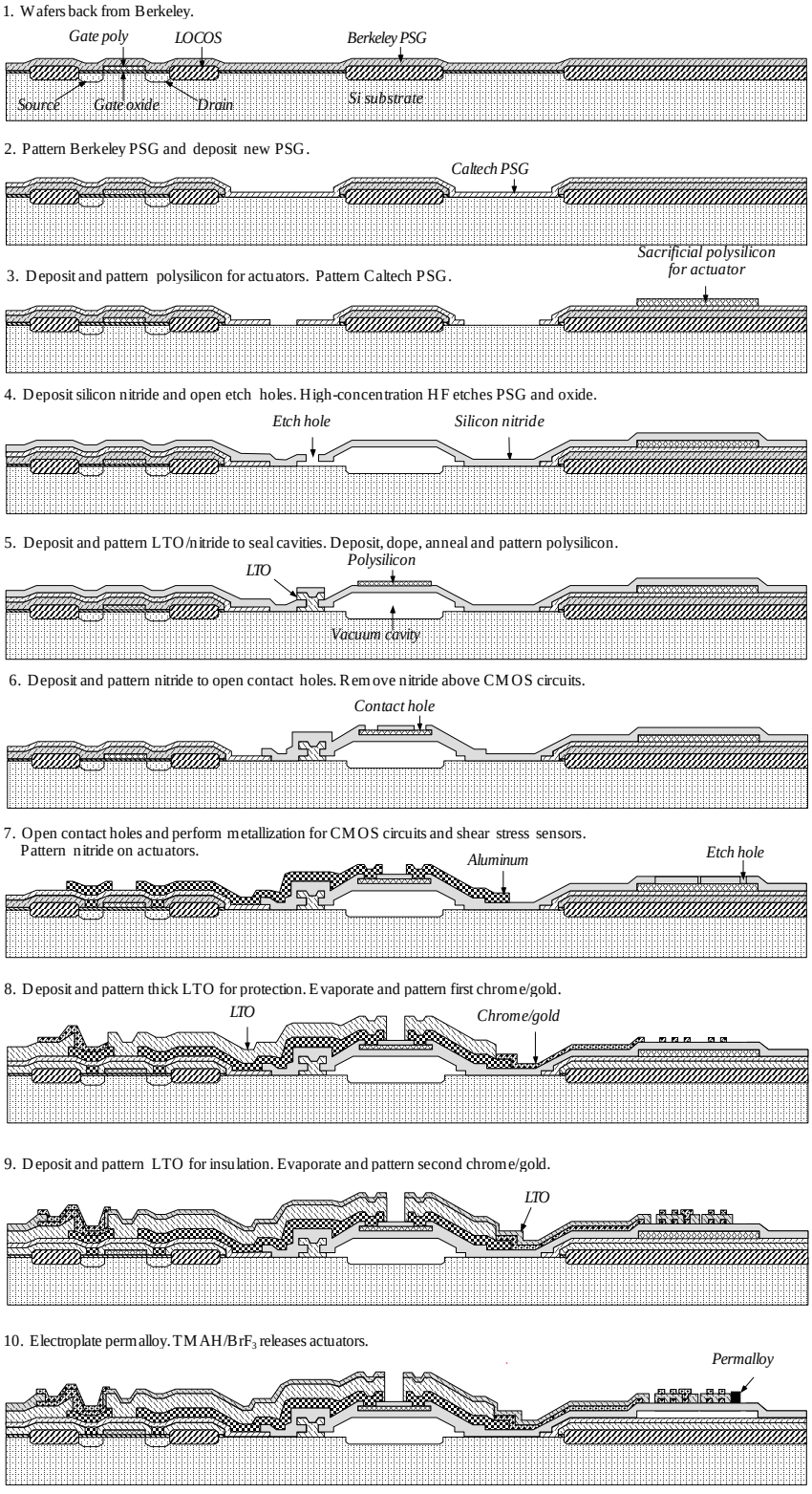

Figure 5.3 Simplified process flow the prototype M^3 chips.

Figure 5.4 shows the picture of a shear stress sensor on the M^3 chips. It is slightly different from sensors on the shear stress imagers. First, the polysilicon wire is chosen to be 15 μm wide so that the voltage drop across the 1:1 Wheatstone bridge in the CT circuit is below 5V. Second, the LOCOS thickness in Berkeley baseline CMOS process is only 0.7 μm, much less than the required 1.8 μm. We have used the 0.7 μm Berkeley PSG to compensate the LOCOS thickness. Meanwhile, we have increased the thickness of our own PSG from 0.4 μm to 0.6 μm in an attempt to further deepen the cavities to the normal 2 μm. However, these were not enough to keep the 1.2 μm thick diaphragms away from the bottom of the vacuum cavities due to the much different boundary conditions (Figure 5.5). It has been found that we need 1.6 μm or thicker diaphragms to prevent them from being sucked down to the cavity bottoms by the vacuum.

The overall wafer surface roughness before the contact hole opening and metallization for the CMOS circuits is about 2.7 μm as a result of lifting the diaphragms above wafer surfaces, which has greatly exceeded the 1 μm limit accepted by the CMOS process vendors who generally use thin photoresist for their UV lithography in order to get fine-line features. Therefore, the lithography for the contact opening and metallization of the CMOS circuits can only be done in our lab using thick photoresist. This would more or less affect the yield of the 2 μm CMOS transistors. Nevertheless, we have found that the test transistors on the wafers with finished shear stress sensors have the same yield (80-90%) as those on the wafers which only went through the complete baseline process in Berkeley Microlab. The threshold voltages of the test transistors on all wafers are about 0.8 V. This means that the additional processing steps at temperatures up to 900^oC did not have significant effect on the performance of the CMOS transistors.

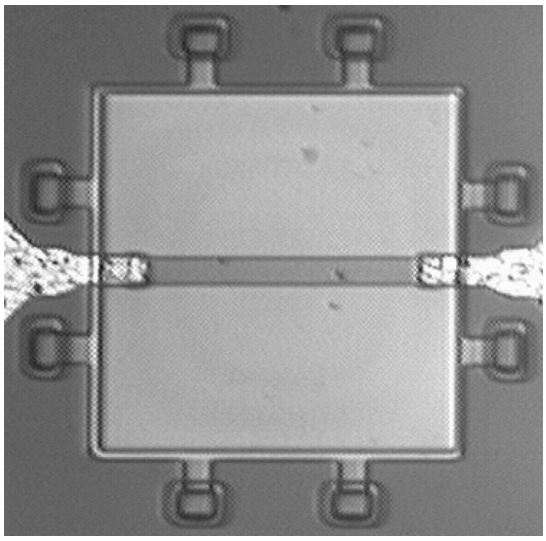

Figure 5.4 Photograph of the low voltage shear stress sensor on a M^3 chip. The polysilicon wire is 15 μm wide and 150 μm long. The Newton rings are the result of the bending on the diaphragm by the vacuum underneath.

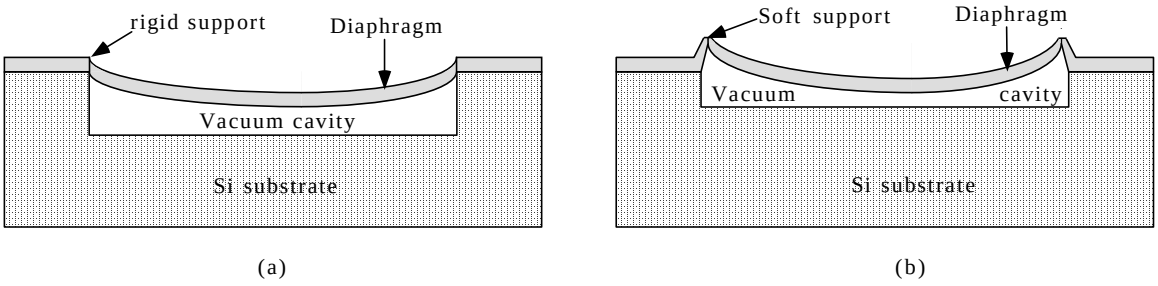

Figure 5.5 Deflection of diaphragms on top of vacuum cavities with (a) rigid and (b) soft supports.

For future efforts on the integration, we need to look into other commercial CMOS process foundries who have better yields and more flexibility in accommodating certain process steps which are important to our MEMS devices but still compatible with the CMOS process. For example, a 1 μm deep fully recessed LOCOS is not difficult to develop and is acceptable to a 2 μm CMOS process, but it can greatly reduce the surface roughness of the shear stress sensors. The proposed cross-sectional design shown in Figure 5.6 has a surface roughness less than 1.4 μm, thus allowing the wafers with

fabricated shear stress sensors to go back to the vendors to finish the remaining CMOS process steps (contact opening and metallization).

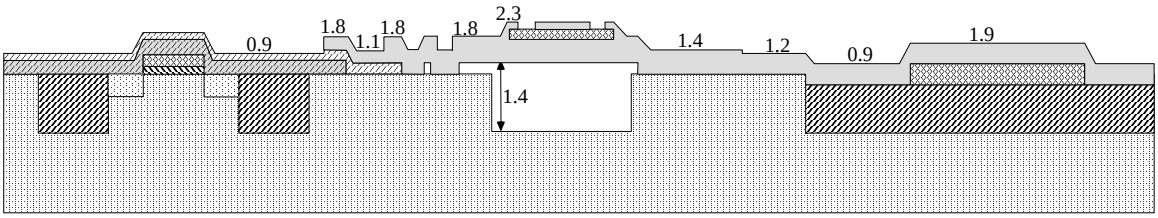

Figure 5.6 The proposed design with 1 μm fully recessed LOCOS and greatly reduced surface roughness. The numbers are the surface levels relative to the silicon surface in unit of microns.

5.4 Conclusion

We have described a novel approach that is capable of controlling turbulent boundary structures and reducing the skin-friction drag through the interaction between the flow and the micro transducers. We have also developed a technology for the integration of micro-sensors, micro-actuators and microelectronics on a single chip (M^3 chip). Prototype M^3 chips designed for the skin-friction drag reduction and consisting of micro shear stress sensors, micro magnetic actuators and CMOS circuits have been fabricated by using this technology. However, some improvements on the design of process, layout and circuits need to be done before we can produce a working M^3 chip for drag reduction.

Bibliography

[1] M. J. Walsh, “Drag Characteristics of V-Groove and Transverse Curvature Riblets,” *Proc. Symp. On Viscous Drag Reduction*, Dallas, 1979.

[2] M. J. Walsh and A. M. Liindermann, “Optimization and Application of Riblets for Turbulent Drag Reduction,” AIAA Paper 84-0347, 1984.

[3] P. Vukoslavcevic, J. M. Wallace, and J. L. Balint, “Viscous Drag Reduction Using Streamwise-Aligned Riblets,” *AIAA J.*, Vol. 30 (4), pp. 1119-1122, 1992.

[4] B. Lazos and P. Wilkinson, “Turbulent Viscous Drag Reduction with Thin-Element Riblets,” *AIAA J.*, Vol. 26 (4), pp. 496-498, 1988.

[5] J. N. Hefner, L. M. Weinstein, and D. M. Bushnell, “Large-Eddy Break-up Scheme for Turbulent Viscous Drag Reduction,” *Proc. Symp. On Viscous Drag Reduction*, Dallas, 1979.

[6] A. P. Dowling, “The Effect of Large-Eddy Breakup Devices on Oncoming Vorticity,” *J. Fluid Mech.*, Vol. 160, pp. 447-463, 1985.

[7] H. Choi, P. Moin, and J. Kim, “Active Turbulence Control For Drag Reduction in Wall-Bounded Flows,” *J. Fluid Mech.*, Vol. 262, pp. 75-110, 1994.

[8] D. W. Bechert, G. Hoppe, and W. E. Reif, “On the Drag Reduction of the Shark Skin,” AIAA Paper 85-0546, 1985.

[9] M. Gad-el-Hak, R. F. Blackwelder, “A Drag Reduction Method for Turbulent Boundary Layers,” AIAA Paper 87-0358, 1987.

[10] S. P. Wilkinson, “Direct Drag Measurements on Thin-Element Riblets with Suction and Blowing,” AIAA Paper 88-3670, 1988.

[11] H. A. Carlson and J. L. Lumley, “Active Control in the Turbulent Wall Layer of a Minimal Flow Unit,” *J. Fluid Mech.*, Vol. 329, pp. 341-371, 1996.

[12] S. P. Wilkinson, “Interactive Wall Turbulence Control,” *Viscous Drag Reduction in Boundary Layers, Progress in Astronautics and Aeronautics*, Vol. 123, pp.479-509, 1989.

[13] R. Miller, Y. C. Tai, G. Burr, D. Psaltis, C. M. Ho, and R. Katti, “Electromagnetic MEMS Scanning Mirrors for Holographic Data Storage,” *Solid-State Sensor and Actuator Workshop*, Hilton Head, SC, pp. 183-186, 1996.

[14] C. H. Ho, S. Tung, and Y. C. Tai, “Interactive Control of Wall Structures by MEMS-Based Transducers,” *Proc. of the Sixth European Turbulence Conference*, Lausanne, Switzerland, p. 413, 1996.

[15] C. H. Ho, S. Tung, G. W. Lee, Y. C. Tai, F. Jiang, T. Tsao, “MEMS - A Technology for Advancements in Aerospace Engineering,” AIAA Paper 97-0545, 1997.

[16] T. Tsao, F. Jiang, R. Miller, Y. C. Tai, B. Gupta, R. Goodman, S. Tung, and C. H. Ho, “An Integrated MEMS System for Turbulent Boundary Layer Control,” *Transducers’97*, Chicago, pp. 315-318, 1997.

[17] B. Gupta, R. Goodman, F. Jiang, Y. C. Tai, S. Tung, and C. H. Ho, “Analog VLSI System for Active Drag Reduction,” *IEEE Micro*, Vol. 16 (5), pp. 53-59, 1996.

[18] B. Gupta, *Analog VLSI for Active Drag Reduction*, Ph. D. Thesis, The California Institute of Technology, 1997.